EUROPEAN ORGANIZATION FOR NUCLEAR RESEARCH

CERN-EP/2003-081
28 November 2003

Flavour independent search for Higgs bosons decaying into hadronic final states in e^+e^- collisions at LEP

The OPAL Collaboration

Abstract

A search for the Higgsstrahlung process $e^+e^- \to hZ$ is described, where the neutral Higgs boson h is assumed to decay into hadronic final states. In order to be sensitive to a broad range of models, the search is performed independent of the flavour content of the Higgs boson decay. The analysis is based on e^+e^- collision data collected by the OPAL detector at energies between 192 GeV and 209 GeV. The search does not reveal any significant excess over the Standard Model background prediction. Results are combined with previous searches at energies around 91 GeV and at 189 GeV. A limit is set on the product of the cross-section and the hadronic branching ratio of the Higgs boson, as a function of the Higgs boson mass. Assuming the hZ coupling predicted by the Standard Model, and a Higgs boson decaying only into hadronic final states, a lower bound of 104 GeV/c^2 is set on the mass at the 95% confidence level.

(Submitted to Physics Letters **B**)

The OPAL Collaboration

G. Abbiendi[2], C. Ainsley[5], P.F. Åkesson[3,y], G. Alexander[22], J. Allison[16], P. Amaral[9], G. Anagnostou[1], K.J. Anderson[9], S. Arcelli[2], S. Asai[23], D. Axen[27], G. Azuelos[18,a], I. Bailey[26], E. Barberio[8,p], T. Barillari[32], R.J. Barlow[16], R.J. Batley[5], P. Bechtle[25], T. Behnke[25], K.W. Bell[20], P.J. Bell[1], G. Bella[22], A. Bellerive[6], G. Benelli[4], S. Bethke[32], O. Biebel[31], O. Boeriu[10], P. Bock[11], J. Böhme[m], M. Boutemeur[31], S. Braibant[8], L. Brigliadori[2], R.M. Brown[20], K. Buesser[25], H.J. Burckhart[8], S. Campana[4], R.K. Carnegie[6], A.A. Carter[13], J.R. Carter[5], C.Y. Chang[17], D.G. Charlton[1], C. Ciocca[2], A. Csilling[29], M. Cuffiani[2], S. Dado[21], A. De Roeck[8], E.A. De Wolf[8,s], K. Desch[25], B. Dienes[30], M. Donkers[6], J. Dubbert[31], E. Duchovni[24], G. Duckeck[31], I.P. Duerdoth[16], E. Etzion[22], F. Fabbri[2], L. Feld[10], P. Ferrari[8], F. Fiedler[31], I. Fleck[10], M. Ford[5], A. Frey[8], P. Gagnon[12], J.W. Gary[4], G. Gaycken[25], C. Geich-Gimbel[3], G. Giacomelli[2], P. Giacomelli[2], M. Giunta[4], J. Goldberg[21], E. Gross[24], J. Grunhaus[22], M. Gruwé[8], P.O. Günther[3], A. Gupta[9], C. Hajdu[29], M. Hamann[25], G.G. Hanson[4], A. Harel[21], M. Hauschild[8], C.M. Hawkes[1], R. Hawkings[8], R.J. Hemingway[6], G. Herten[10], R.D. Heuer[25], J.C. Hill[5], A. Hocker[34] K. Hoffman[9], D. Horváth[29,c], P. Igo-Kemenes[11], K. Ishii[23], H. Jeremie[18], P. Jovanovic[1], T.R. Junk[6,i], N. Kanaya[26], J. Kanzaki[23,u], D. Karlen[26], K. Kawagoe[23], T. Kawamoto[23], R.K. Keeler[26], R.G. Kellogg[17], B.W. Kennedy[20], K. Klein[11,t], A. Klier[24], S. Kluth[32], T. Kobayashi[23], M. Kobel[3], S. Komamiya[23], T. Krämer[25], P. Krieger[6,l], J. von Krogh[11], K. Kruger[8], T. Kuhl[25], M. Kupper[24], G.D. Lafferty[16], H. Landsman[21], D. Lanske[14], J.G. Layter[4], D. Lellouch[24], J. Letts[o], L. Levinson[24], J. Lillich[10], S.L. Lloyd[13], F.K. Loebinger[16], J. Lu[27,w], A. Ludwig[3], J. Ludwig[10], W. Mader[3], S. Marcellini[2], A.J. Martin[13], G. Masetti[2], T. Mashimo[23], P. Mättig[m], J. McKenna[27], R.A. McPherson[26], F. Meijers[8], W. Menges[25], F.S. Merritt[9], H. Mes[6,a], A. Michelini[2], S. Mihara[23], G. Mikenberg[24], D.J. Miller[15], S. Moed[21], W. Mohr[10], T. Mori[23], A. Mutter[10], K. Nagai[13], I. Nakamura[23,v], H. Nanjo[23], H.A. Neal[33], R. Nisius[32], S.W. O'Neale[1], A. Oh[8], A. Okpara[11], M.J. Oreglia[9], S. Orito[23,*], C. Pahl[32], G. Pásztor[4,g], J.R. Pater[16], J.E. Pilcher[9], J. Pinfold[28], D.E. Plane[8], B. Poli[2], O. Pooth[14], M. Przybycień[8,n], A. Quadt[3], K. Rabbertz[8,r], C. Rembser[8], P. Renkel[24], J.M. Roney[26], S. Rosati[3,y], Y. Rozen[21], K. Runge[10], K. Sachs[6], T. Saeki[23], E.K.G. Sarkisyan[8,j], A.D. Schaile[31], O. Schaile[31], P. Scharff-Hansen[8], J. Schieck[32], T. Schörner-Sadenius[8,a1], M. Schröder[8], M. Schumacher[3], W.G. Scott[20], R. Seuster[14,f], T.G. Shears[8,h], B.C. Shen[4], P. Sherwood[15], A. Skuja[17], A.M. Smith[8], R. Sobie[26], S. Söldner-Rembold[15], F. Spano[9], A. Stahl[3,x], D. Strom[19], R. Ströhmer[31], S. Tarem[21], M. Tasevsky[8,z], R. Teuscher[9], M.A. Thomson[5], E. Torrence[19], D. Toya[23], P. Tran[4], I. Trigger[8], Z. Trócsányi[30,e], E. Tsur[22], M.F. Turner-Watson[1], I. Ueda[23], B. Ujvári[30,e], C.F. Vollmer[31], P. Vannerem[10], R. Vértesi[30,e], M. Verzocchi[17], H. Voss[8,q], J. Vossebeld[8,h], D. Waller[6], C.P. Ward[5], D.R. Ward[5], P.M. Watkins[1], A.T. Watson[1], N.K. Watson[1], P.S. Wells[8], T. Wengler[8], N. Wermes[3], D. Wetterling[11] G.W. Wilson[16,k], J.A. Wilson[1], G. Wolf[24], T.R. Wyatt[16], S. Yamashita[23], D. Zer-Zion[4], L. Zivkovic[24]

[1]School of Physics and Astronomy, University of Birmingham, Birmingham B15 2TT, UK
[2]Dipartimento di Fisica dell' Università di Bologna and INFN, I-40126 Bologna, Italy

[3]Physikalisches Institut, Universität Bonn, D-53115 Bonn, Germany
[4]Department of Physics, University of California, Riverside CA 92521, USA
[5]Cavendish Laboratory, Cambridge CB3 0HE, UK
[6]Ottawa-Carleton Institute for Physics, Department of Physics, Carleton University, Ottawa, Ontario K1S 5B6, Canada
[8]CERN, European Organisation for Nuclear Research, CH-1211 Geneva 23, Switzerland
[9]Enrico Fermi Institute and Department of Physics, University of Chicago, Chicago IL 60637, USA
[10]Fakultät für Physik, Albert-Ludwigs-Universität Freiburg, D-79104 Freiburg, Germany
[11]Physikalisches Institut, Universität Heidelberg, D-69120 Heidelberg, Germany
[12]Indiana University, Department of Physics, Bloomington IN 47405, USA
[13]Queen Mary and Westfield College, University of London, London E1 4NS, UK
[14]Technische Hochschule Aachen, III Physikalisches Institut, Sommerfeldstrasse 26-28, D-52056 Aachen, Germany
[15]University College London, London WC1E 6BT, UK
[16]Department of Physics, Schuster Laboratory, The University, Manchester M13 9PL, UK
[17]Department of Physics, University of Maryland, College Park, MD 20742, USA
[18]Laboratoire de Physique Nucléaire, Université de Montréal, Montréal, Québec H3C 3J7, Canada
[19]University of Oregon, Department of Physics, Eugene OR 97403, USA
[20]CCLRC Rutherford Appleton Laboratory, Chilton, Didcot, Oxfordshire OX11 0QX, UK
[21]Department of Physics, Technion-Israel Institute of Technology, Haifa 32000, Israel
[22]Department of Physics and Astronomy, Tel Aviv University, Tel Aviv 69978, Israel
[23]International Centre for Elementary Particle Physics and Department of Physics, University of Tokyo, Tokyo 113-0033, and Kobe University, Kobe 657-8501, Japan
[24]Particle Physics Department, Weizmann Institute of Science, Rehovot 76100, Israel
[25]Universität Hamburg/DESY, Institut für Experimentalphysik, Notkestrasse 85, D-22607 Hamburg, Germany
[26]University of Victoria, Department of Physics, P O Box 3055, Victoria BC V8W 3P6, Canada
[27]University of British Columbia, Department of Physics, Vancouver BC V6T 1Z1, Canada
[28]University of Alberta, Department of Physics, Edmonton AB T6G 2J1, Canada
[29]Research Institute for Particle and Nuclear Physics, H-1525 Budapest, P O Box 49, Hungary
[30]Institute of Nuclear Research, H-4001 Debrecen, P O Box 51, Hungary
[31]Ludwig-Maximilians-Universität München, Sektion Physik, Am Coulombwall 1, D-85748 Garching, Germany
[32]Max-Planck-Institute für Physik, Föhringer Ring 6, D-80805 München, Germany
[33]Yale University, Department of Physics, New Haven, CT 06520, USA
[34]University of Rochester, Rochester, New York 14627, USA

[a] and at TRIUMF, Vancouver, Canada V6T 2A3
[c] and Institute of Nuclear Research, Debrecen, Hungary
[e] and Department of Experimental Physics, University of Debrecen, Hungary
[f] and MPI München
[g] and Research Institute for Particle and Nuclear Physics, Budapest, Hungary
[h] now at University of Liverpool, Dept of Physics, Liverpool L69 3BX, U.K.

[i] now at Dept. Physics, University of Illinois at Urbana-Champaign, U.S.A.
[j] and Manchester University
[k] now at University of Kansas, Dept of Physics and Astronomy, Lawrence, KS 66045, U.S.A.
[l] now at University of Toronto, Dept of Physics, Toronto, Canada
[m] current address Bergische Universität, Wuppertal, Germany
[n] now at University of Mining and Metallurgy, Cracow, Poland
[o] now at University of California, San Diego, U.S.A.
[p] now at Physics Dept Southern Methodist University, Dallas, TX 75275, U.S.A.
[q] now at IPHE Université de Lausanne, CH-1015 Lausanne, Switzerland
[r] now at IEKP Universität Karlsruhe, Germany
[s] now at Universitaire Instelling Antwerpen, Physics Department, B-2610 Antwerpen, Belgium
[t] now at RWTH Aachen, Germany
[u] and High Energy Accelerator Research Organisation (KEK), Tsukuba, Ibaraki, Japan
[v] now at University of Pennsylvania, Philadelphia, Pennsylvania, USA
[w] now at TRIUMF, Vancouver, Canada
[x] now at DESY Zeuthen
[y] now at CERN
[z] now with University of Antwerp
[a1] now at DESY
[*] Deceased

1 Introduction

In the Standard Model (SM) and for masses relevant to the LEP energy range, the Higgs boson is predicted to be produced principally by the Higgsstrahlung process $e^+e^- \to hZ$ and to decay dominantly into the $b\bar{b}$ channel. This is also the case in large domains of the Minimal Supersymmetric Standard Model (MSSM) parameter space (the Higgs phenomenology is reviewed, e.g. in Ref. [1]). Most of the searches conducted so far at LEP, therefore, tag the b flavour to enhance the Higgs boson signal.

In other scenarios, however, the decay of the Higgs boson into lighter quark flavours or into gluon pairs may be important. Such is the case in general models with two Higgs field doublets (2HDM) [1, 2] or other extended models [3]. In order to be sensitive to Higgs bosons predicted by such models, the search described here is based only on kinematic selections which are insensitive to the hadron flavour present in the final state. Such searches have already been reported by OPAL; these were based on data collected at energies close to the Z boson resonance [4] and at a centre-of-mass energy ($\sqrt{s}$) of 189 GeV [5]. A similar search has also been reported by ALEPH [6].

This paper describes a flavour independent search which is based on OPAL data collected at centre-of-mass energies between 192 and 209 GeV with an integrated luminosity of about 420pb^{-1}. For the results presented, this search is combined with the earlier OPAL searches [4, 5].

2 Data sets and Monte Carlo simulation

The OPAL detector is described in Ref. [7]. The events selected for the analysis have to satisfy a set of detector status requirements which ensure that all relevant detector elements are active. Events are reconstructed from charged particle tracks observed in the central tracking detector and energy deposits ("clusters") in the electromagnetic and hadron calorimeters. The tracks and clusters are required to pass a set of quality requirements [8]. In calculating the visible energies and momenta $E_{\rm vis}$ and $\vec{P}_{\rm vis}$, either for individual jets or for the events, corrections are applied to prevent double-counting of the energy attributed to the tracks and to the clusters geometrically associated to the tracks [9].

The data sets to which the present analysis applies were collected in 1999 at $\sqrt{s}$ between 192 and 202 GeV and in the year 2000 at $\sqrt{s}$ between 200 and 209 GeV. After the detector status requirements the data sample has an integrated luminosity of approximately 420pb^{-1}. The exact amount varies among the different channels (see Table 1).

A variety of Monte Carlo samples have been generated to estimate the selection efficiencies for the Higgs boson signal and for the background processes. In order to cover the range of energies of the data, the simulations are performed at fixed values of $\sqrt{s}$ between 192 and 210 GeV and for a set of Higgs boson masses. Spline fits are used to calculate the signal efficiencies at intermediate values.

The Higgsstrahlung process is modelled with the HZHA generator [10]. Samples of 1000 to 5000 events were produced at fixed masses, between 30 and 120 GeV/c^2. The Higgs boson is required to decay, either according to the SM, or separately to $\rm c\bar{c}$, $\rm s\bar{s}$or to pairs of gluons.

The simulated background samples typically have more than 30 times the statistics of the collected data. The following event generators are used: KK2F [11] and PYTHIA [12] for the process $\rm q\bar{q}(\gamma)$, grc4f [13], KORALW [14] and EXCALIBUR [15] for the four-fermion processes, BHWIDE [16] for $\rm e^+e^-(\gamma)$, KORALZ [17] for $\mu^+\mu^-(\gamma)$ and $\tau^+\tau^-(\gamma)$, and PHOJET [18], HERWIG [19] and VERMASEREN [20] for hadronic and leptonic two-photon processes and for $\rm e^+e^- \to e^+e^-\gamma\gamma$. Hadronisation is modelled with JETSET [12] using parameters described in [21]. The cluster fragmentation model in HERWIG is used to study the uncertainties due to quark and gluon jet fragmentation. The Monte Carlo samples pass through a detailed simulation of the OPAL detector [22] and are subjected to the same analysis procedure as applied to the data.

3 Analysis

The search described in this paper addresses the Higgsstrahlung process $\rm e^+e^- \to hZ$. The neutral Higgs boson h is assumed to decay into quark pairs of arbitrary flavour or into gluon pairs. The following hZ final states (search channels) are therefore considered,

depending on the decay of the Z boson: the four-jet channel ($Z \to q\bar{q}$), the missing energy channel ($Z \to \nu\bar{\nu}$) and the electron, muon and tau channels ($Z \to e^+e^-$, $\mu^+\mu^-$ and $\tau^+\tau^-$).

The analysis assumes that the decay width of the Higgs boson is within the range $10^{-4} < \Gamma_h < 1$ GeV/c^2. This ensures that the decay of the Higgs boson occurs within about 1 mm of the e^+e^- interaction point and that the reconstructed Higgs boson mass has a width that is dominated by the experimental resolution, between 2 and 5 GeV/c^2, depending on the search channel. The search strategies are similar to those applied by OPAL in the search for the SM Higgs boson [23] (see Ref. [24] for the missing energy channel) except that the b-tagging requirements are replaced by more elaborate kinematic selections.

In the searches addressing each of the final states, a preselection is applied first which strongly reduces the background while maintaining a high signal detection efficiency. The preselected events are then submitted to a likelihood test, which discriminates between the signal and the two most important background sources, 2-fermion and 4-fermion processes. Other background processes, in particular 2-photon events, are negligible after the first preselection cuts (see Section 3 of [23]). The likelihood function is constructed from reference distributions of a number of discriminating variables which are obtained from detailed simulations of the signal and background processes. In the four-jet channel, these distributions are obtained from a three-dimensional spline fit to the distributions of simulated events where the dimensions are $\sqrt{s}$, the hypothetic Higgs boson mass (test-mass) and the variable itself.

Finally, a cut is applied on the value of this likelihood function. For each of the search channels, the effect of the preselection and likelihood cuts on the data samples, the total background and its contributions, and on the signal detection efficiency for two test-masses can be followed through Table 1.

The signal efficiency is evaluated separately for each of the $h \to b\bar{b}$, $c\bar{c}$, $s\bar{s}$ and gg decay hypotheses. At a given test-mass, these efficiencies typically vary by about $\pm 5\%$. This is illustrated in Figure 1(a) for the search in the four-jet channel. In deriving flavour independent bounds on the hZ coupling, the smallest of these efficiencies is used; it is obtained for $h \to$ gg in the four-jet and tau channels and for $h \to c\bar{c}$ or $b\bar{b}$ in the missing energy and lepton channels. For the decays into light flavours, $h \to u\bar{u}$ and $d\bar{d}$, the efficiencies are slightly higher since the jets are better collimated and because weak semileptonic decays are absent; this has been verified explicitly using $e^+e^- \to ZZ$ events. These minimal efficiencies are shown for all but the four-jet search by the curves in Figure 1(b).

3.1 Search in the four-jet channel

In the four-jet channel the main background arises from the $e^+e^- \to WW$ process. Further contributions are from $e^+e^- \to (Z/\gamma)^* \to q\bar{q}$ and $e^+e^- \to ZZ$. The analysis described below is repeated for fixed test-masses, in steps of 250 MeV/c^2, between 60 and 120 GeV/c^2. The following preselection is applied:

1. Events must be identified as multihadronic final states [25].

Cut	Data	Total bkg.	$q\bar{q}(\gamma)$	4–fermi.	Efficiency in % 90 GeV/c^2	100 GeV/c^2
Four–jet Channel Luminosity = 424.3pb^{-1}						
(1)	39090	38831.1	29929.3	8322.0	100	100
(2)	13692	13648.5	8602.5	5012.2	100	100
(3)	4645	4504.3	1077.9	3418.4	93	95
(4)	4200	4038.4	932.7	3105.7	92	94
(5)	3695	3561.3	603.2	2958.1	90	91
(6)	3594	3447.2	581.2	2866.0	89	90
(7)	2535	2399.6	504.2	1895.4	81	83
(8)	2081	1975.3	477.2	1498.1	78	80
(9)	659	637.4	155.8	481.6	59	66
$\mathcal{L}$	439	414.0	103.8	136.0	52	54
Missing–energy Channel Luminosity = 420.9pb^{-1}						
(1)	9040	8524.6	6063.7	2382.4	87	78
(2)	2615	2391.3	686.0	1691.2	80	73
(3)	2462	2289.9	665.4	1614.6	77	73
(4)	1635	1598.4	110.7	1487.7	72	69
(5)	650	605.4	48.5	556.8	70	67
(6)	298	291.4	42.3	249.1	65	62
$\mathcal{L}$	123	133.1	6.3	126.6	45	48
Electron Channel Luminosity = 422.3pb^{-1}						
(1)	18042	18221.3	12176.4	6045.0	92	97
(2)	558	538.7	252.8	286.1	75	78
(3)	429	378.6	171.0	207.6	74	78
$\mathcal{L}$	23	16.6	0.2	16.3	59	59
Muon Channel Luminosity = 421.4pb^{-1}						
(1)	18008	18184.6	8715.5	9469.0	88	92
(2)	505	477.5	236.5	241.0	77	81
(3)	79	66.1	32.6	33.6	74	75
$\mathcal{L}$	16	15	6.6	8.4	64.8	62.4
Tau Channel Luminosity = 409.0pb^{-1}						
(1)	10417	10082	5520.1	4561.8	83	78
(2)	1652	1687.6	187.0	1500.9	62	61
(3)	418	404.5	99.5	305.2	48	47
(4)	358	343.1	96.6	246.3	47	47
$\mathcal{L}$	3	8.8	0.23	8.57	27	21

Table 1: Number of events selected in the different search channels after consecutive cuts. In each case, the final likelihood cut is denoted by $\mathcal{L}$. The number of events found in the data is compared to the expectation from simulations. In the four-jet channel the numbers up to and including cut (8) are valid for all test-masses; those for cut (9) and the final likelihood cut are given for a test-mass of 100 GeV/c^2. The last two columns show the evolution of the selection efficiencies for Higgs bosons of 90 GeV/c^2 and 100 GeV/c^2 mass decaying exclusively into hadronic final states at 196 and 206 GeV centre-of-mass energy, respectively.

2. The effective centre-of-mass energy $\sqrt{s'}$ (disregarding initial-state photon radiation, see Ref. [25]), is required to exceed 80% of the total centre-of-mass energy.

3. Events are forced into four jets using the Durham algorithm [26] and are selected if the resolution parameter y_{34} is larger than $3 \cdot 10^{-3}$.

4. Each of the jets must contain at least two charged particle tracks to suppress events with isolated leptons or photons, like $e^+e^- \to q\bar{q}\ell^+\ell^-$.

5. The matrix element ME_{QCD} for the QCD-induced processes $e^+e^- \to q\bar{q}q\bar{q}$ and $e^+e^- \to q\bar{q}gg$ is calculated [27], approximating the parton momenta by the reconstructed jet momenta. The matrix element averaged over all possible flavour combinations is required to be within the range $-3 < \ln|ME_{QCD}| < -1$.

6. The χ^2-probability resulting from a four-constraint (4C) kinematic fit which imposes energy and momentum conservation is required to be larger than 10^{-6}.

7. The four-fermion background is reduced by a cut on the matrix element ME_{4f} of the process $e^+e^- \to q\bar{q}q\bar{q}$, calculated using EXCALIBUR [15]. In the calculation the parton momenta are approximated by the jet momenta resulting from the 4C fit and the matrix element is averaged over all flavour combinations. Its value is required to be within the range $-8.5 < \ln|ME_{4f}| < -4.9$.

8. The WW $\to$ hadrons hypothesis is tested in a kinematic 6C fit imposing energy and momentum conservation and where the invariant masses of the two jet pairs are constrained to the W boson mass. To suppress the WW background, the largest of the χ^2-probabilities, $P^{max}(WW)$, for the three possible jet pairings is required to be less than 6.3%.

9. Finally, for each value of the test-mass, a kinematic fit is performed imposing energy and momentum conservation and constraining one dijet mass to the test-mass and the other to the Z boson mass. In the fit, the reconstructed Z boson mass is allowed to vary within its natural width according to a Gaussian distribution[1]. The largest of the χ^2-probabilities $P^{max}(Zh)$ resulting from the six possible jet assignments to the Z and the h bosons is required to exceed 10^{-6}.

The signal likelihood is constructed using the following 6 variables: (1) the maximum probability $P^{max}(hZ)$ of the hZ kinematic fit; (2) the Higgsstrahlung matrix element ME_{hZ} [28] for the test-mass considered and for the jet combination which yields $P^{max}(hZ)$; the ratios (3) ME_{hZ}/ME_{4f} and (4) ME_{hZ}/ME_{QCD}; (5) the difference between the maximum and minimum energies of the four jets after the 4C kinematic fit; and (6) $P^{max}(WW)$. Distributions of these input variables are presented in Figure 2, while the likelihood distributions for two test-masses are shown in Figure 3 (a) and (b). Events with a likelihood larger than 0.1 are accepted.

The signal efficiency and residual background rates are affected by the following systematic uncertainties: (a) Uncertainties in modelling of the momenta, the angular and energy resolutions and the energy scale of the reconstructed jets are less than 2% for both

[1]The sensitivity of the search would be slightly lower if a Breit-Wigner distribution were used.

the signal efficiency and the background rate. They have been determined by comparing calibration data taken at the Z resonance to the Monte Carlo simulation and transferring the observed differences to the simulation of the high energy data. (b) Uncertainties in modelling the preselection and likelihood variables are less than 3% for the signal and $4-9\%$ for the background, depending on the test-mass. Weights were applied to the simulated events such that a $\chi^2 < 1$ is obtained when comparing the shapes of the distributions from the data and the simulation of the background (for each variable separately). The difference of the signal efficiency and background of the weighted and unweighted events is considered as the systematic error. It has been explicitly checked that a hypothetical signal is not hidden by this procedure. (c) Using alternatively JETSET and HERWIG to simulate hadron fragmentation yields a difference of $2-13\%$ for the background. (d) The cross-section of the four-fermion processes, which dominates the residual background, is known to within 2% [30]. (e) Monte Carlo statistics contribute $1-5\%$ for the signal and less than 3% for the background. Combining all these effects, the total systematic uncertainty amounts to less than 6% for the signal efficiency and $5-16\%$ for the residual background.

The number of selected events in the four-jet channel with a likelihood value larger than 0.5 is shown in Figure 4 (a) for test-masses between 60 and 120 GeV/c^2. The selected data samples for mass hypotheses which differ by less than the mass resolution (of about 5 GeV/c^2 at high likelihood values) are strongly correlated. For a test-mass of 100 GeV/c^2, 439 candidates pass the final likelihood cut of 0.1 while 414 ± 53 events are expected from background processes and 40 events would be expected from Higgsstrahlung if the hZ coupling predicted by the SM is assumed and the Higgs boson decays only into hadronic final states. The signal to background ratio becomes more favourable for larger likelihood values.

3.2 Search in the missing energy channel

Signal events in the missing energy channel are characterised by two hadronic jets and a missing mass consistent with the Z boson mass. The dominant backgrounds are four-fermion processes, in particular from the semi-leptonic decays $e^+e^- \to WW \to q\bar{q}\ell^{\pm}\nu$, and the irreducible process $e^+e^- \to ZZ \to \nu\bar{\nu}q\bar{q}$. Further contributions are from events with particles escaping detection along the beam-pipe, for example from Z boson decays accompanied by initial-state photons or the untagged two-photon process $e^+e^- \to e^+e^-q\bar{q}$. The following preselection is applied:

1. To reject non-hadronic events, at least 7 charged particle tracks are required. At least 20% of all tracks must be of good quality (a minimum number of hits are required along the track, see Ref. [8]); this is to reject badly measured events, mainly two-photon processes and beam-wall interactions. The total transverse momentum p_t and the visible mass $m_{\rm vis}$ must satisfy $5 \times p_t + m_{\rm vis} > \sqrt{s}/2$, and the visible energy $E_{\rm vis} < 0.8\sqrt{s}$. The energy measured in the forward detector components [7], which cover small polar angles, must be < 2 GeV in the forward calorimeters, < 5 GeV in the gamma catcher and < 5 GeV in the silicon-tungsten calorimeter [32]. The overall energy observed in the region $|\cos\theta| > 0.9$, where θ denotes the polar angle with respect to the electron beam, must not exceed 20% of $E_{\rm vis}$.

2. The missing momentum vector has to point to sensitive parts of the detector, $|\cos\theta_{\rm miss}| < 0.95$, and the visible momentum must not have a large component along the beam axis, $|p^z_{\rm vis}| < \sqrt{s}/5$.

3. The tracks and clusters in each event are forced into two jets using the Durham algorithm. Events with partially contained jets are rejected by the requirement $|\cos\theta_{\rm jet}| < 0.95$ imposed on each jet.

4. $(\mathrm{Z}/\gamma)^* \rightarrow \mathrm{q\bar{q}}$ events are suppressed by requesting $\phi_{\rm acop} > 5^\circ$ where the acoplanarity angle $\phi_{\rm acop}$ is the deviation of the angle between the two jets in the plane perpendicular to the beam axis from 180°.

5. The missing mass, $m_{\rm miss}$, must be consistent with the Z boson mass: $50\ \mathrm{GeV/c^2} < m_{\rm miss} < 130\ \mathrm{GeV/c^2}$.

6. Identified semi-leptonic WWdecays with energetic, isolated [32] leptons are discarded.

The signal likelihood function is constructed from 5 variables: (1) $m_{\rm miss}$; (2) $|\cos\theta_{\rm miss}|$; (3) $\max|\cos\theta_{\rm jet}|$ i.e. the polar angle of the jet closest to the beam axis; (4) the χ^2-probability P(1C) of a one-constraint (1C) kinematic fit which imposes energy and momentum conservation and constrains the missing mass to the Z boson mass; (5) the angle between the missing momentum and the jet with the higher energy: $\cos\theta_{\rm j-miss}$. The distributions of these discriminating variables are shown in Figure 5 and the likelihood distribution in Figure 3 (c). Events with a likelihood larger than 0.4 are selected. The Higgs boson mass is reconstructed using the momenta provided by the 1C kinematic fit.

The number of events passing the likelihood selection is 123 (see Table 1) while 133±11 events are expected from SM background processes. The most important systematic uncertainties [24] are from the modelling of the likelihood input variables and from the lepton isolation criteria. The signal efficiencies are affected by a total systematic error of 2.9%. The Monte Carlo estimates of the signal efficiencies were reduced by 2.5% to account for accidental vetoes due to accelerator-related backgrounds in the forward detectors. The reduction factor was determined from randomly triggered events.

3.3 Searches in the electron and muon channels

The signal events in the muon and electron channels are expected to have two energetic, oppositely charged, isolated leptons and two hadronic jets. The dominant backgrounds are $\mathrm{e^+e^-} \rightarrow (\mathrm{Z}/\gamma)^*$ accompanied by initial state radiation and four-fermion processes, mainly from WW and ZZ pairs. The preselection is described in the following:

1. Events without hadronic jets are rejected by requiring at least 6 charged particle tracks. The visible energy $E_{\rm vis}$ must be larger than $0.6\sqrt{s}$ and the component of the total momentum along the beam axis must satisfy $|p^z_{\rm vis}| < E_{\rm vis} - 0.5\sqrt{s}$. This requirement reduces $\mathrm{e^+e^-} \rightarrow (\mathrm{Z}/\gamma)^*\gamma \rightarrow \mathrm{q\bar{q}}\gamma$ and two-photon processes, $\mathrm{e^+e^-} \rightarrow \mathrm{e^+e^-q\bar{q}}$,

significantly. All remaining events are forced into four jets using the Durham algorithm allowing isolated leptons to form low-multiplicity jets. Events are considered further if the jet resolution parameter y_{34} is larger than 10^{-4}.

2. Two oppositely charged electron or muon candidates must be identified, with energies larger than 30 (20) GeV for the higher- (lower-) energy candidate. The energy of muon candidates is deduced from the momentum measurement in the central tracking chamber; for electron candidates the energy measured in the electromagnetic calorimeter is used. The algorithms to identify muons and electrons are described in [31] and [32], respectively.

3. The remaining part of the event, after the two lepton candidates are removed, is reconstructed as a two-jet event using the Durham algorithm. If the lepton candidates are muons, a 4C kinematic fit requiring energy and momentum conservation is performed to improve the energy and mass resolution of the muon pair; the χ^2-probability of the fit must exceed 10^{-5}. For both electron and muon candidate events, the invariant mass of the lepton pair is required to be larger than 40 GeV/c^2.

The signal likelihood is constructed from five variables in the muon channel and nine variables in the electron channel. Those in common are: (1) $E_{\rm vis}/\sqrt{s}$; (2) $\log_{10} y_{34}$; (3-4) the measured transverse momenta of the two lepton candidates ordered by energy and calculated with respect to the nearest jet axis, used to discriminate against semileptonic charm or bottom decays; (5) the invariant mass of the lepton pair. For each candidate in the electron channel, the additional variables are: (6-7) $(E/p-1)/\sigma$ for the two electron candidates, where the momentum p is measured in the central tracking detector, the energy E is measured using the calorimeter and σ denotes the total error in E/p; (8-9) the normalised ionisation energy losses in the central tracking chamber gas [24], for the two electron candidates. The event is selected if in the electron case the likelihood is larger than 0.3 or in the muon case larger than 0.65. Figures 3 (d) and (e) show the distribution of the two likelihood functions. The mass recoiling against the lepton pair is taken as the reconstructed Higgs boson mass.

The number of events passing the likelihood selection is 23 in the electron channel and 16 in the muon channel (see Table 1) while the corresponding background expectations are 16.6 ± 5.1 and 15.0 ± 2.9 events. Systematic uncertainties [24] arise mainly from the fragmentation process, determined from a comparison of HERWIG and JETSET, and from different four-fermion rate predictions, given by grc4f, KORALW and EXCALIBUR. The signal efficiencies have total systematic errors of less than 2% .

3.4 Search in the tau channel

Signal events are expected to be composed of two hadronic jets from the Higgs boson decay, and two tau leptons from the Z decay. For each of the tau leptons, the decays into one or three charged particle tracks ("prongs") are considered, possibly accompanied by calorimeter clusters from neutral particles. Important sources of background are the processes $e^+e^- \to ZZ^{(*)} \to q\bar{q}\ell^+\ell^-$, $e^+e^- \to WW \to q\bar{q}\ell^\pm\nu$ and $e^+e^- \to q\bar{q}(\gamma)$. The following preselection is applied:

1. Events must be identified as multihadronic final states [25]. The visible energy has to exceed $0.3\sqrt{s}$. In order to reject events in which particles escape detection close to the beam direction, the missing momentum vector is required to point to sensitive detector regions: $|\cos\theta_{\rm miss}| < 0.95$. The scalar sum of the transverse momenta of all measured particles has to be larger than 45 GeV/c.

2. Two isolated tau lepton candidates, each with a momentum between 15 GeV/c and 60 GeV/c, are required. These are identified with artificial neural networks (ANN) as described in [24]. Separate networks are developed for 1-prong and 3-prong decays. From the ANN output, the probability that a candidate is a real tau lepton is derived. The probabilities $P_{1,2}$ of the two tau candidates are combined to a two-tau-likelihood: $\mathcal{L}_{\tau\tau} = P_1P_2/(P_1P_2 + (1-P_1)(1-P_2))$, which must exceed 0.1. If several tau pairs exist in the event, the pair with the largest $\mathcal{L}_{\tau\tau}$ is chosen.

3. After removing the two tau candidates, the rest of the event is grouped into two jets using the Durham algorithm. A kinematic fit (2C) is applied to the momenta of the two tau candidates and the two reconstructed jets, imposing energy and momentum conservation. The directions of the tau candidates are approximated by the visible momenta of their decay products; their energies are free parameters in the fit. The χ^2-probability of the fit must be larger than 10^{-5}.

4. If both tau decays are classified as 1-prong decays, the momentum sum of both charged tracks must be less than 80 GeV/c; this is to reduce backgrounds from $\mathrm{e^+e^-} \to \mathrm{ZZ} \to \mathrm{q\bar{q}}\mu^+\mu^-$ and $\mathrm{q\bar{q}e^+e^-}$.

The signal likelihood is constructed using nine variables: (1) the visible energy; (2) $|\cos\theta_{\rm miss}|$; (3) y_{34} obtained after reconstructing the event, including the tracks and clusters of the tau candidates, into four jets (the Durham algorithm is used); (4-5) the angles between each of the two tau candidates and the nearest jet; (6) the energy of the most energetic muon or electron, if any; (7) the χ^2-probability of a 3C kinematic fit, which in comparison to the 2C fit, in addition constrains the invariant mass of the two tau candidates to the Z boson mass; (8) the two-tau likelihood $\mathcal{L}_{\tau\tau}$; (9) the impact parameter joint probability of the tau candidate tracks calculated as in Ref. [29]. The resulting likelihood distribution is shown in Figure 3 (f). Events with a likelihood larger than 0.8 are accepted. The invariant mass of the two jets, resulting from the 3C-fit, is taken as the reconstructed Higgs boson mass.

Three events pass the likelihood cut (see Table 1) compared to 8.8 ± 1.5 events expected from background. The systematic errors are determined as described in [24]. The largest uncertainty arises from the purity of the tau lepton selection. The signal efficiencies are affected by a total systematic error of $15-17\%$.

4 Results

All search channels combined, 604 candidates are selected, while 588 ± 56 are expected from background processes (these numbers apply for a test-mass of 100 GeV/c^2 in the

four-jet channel). Figure 4 (b) shows the distribution of the reconstructed Higgs boson mass for the candidates selected in the missing energy, electron, muon and tau channels, and for the corresponding expected backgrounds, added together.

No significant excess is observed in any of the search channels over the expected background from SM processes. In the following, an upper limit is set on the product of the cross-section σ_{hZ} of the Higgsstrahlung process and the hadronic branching ratio $\mathrm{Br}(\mathrm{h} \to \mathrm{hadrons})$ of the Higgs boson. For this purpose, these search results are combined with previous OPAL results, obtained at $\sqrt{s} = 91$ GeV in the missing energy, electron and muon channels [4], and at $\sqrt{s} = 189$ GeV in all channels [5].

The limits are obtained by using a weighted event counting method (see Section 5 of [33]). The systematic errors are incorporated following Ref. [34]. The four analyses are split into several sub-channels denoted by i depending on the value of the discriminating variable. Initially the weight, $\omega_i = s_i \ / \ (s_i + b_i)$, is assigned to each channel, where s_i and b_i are the signal and background expectation, respectively. These weights are a good choice if the systematic errors are negligible or do not differ among the channels. To obtain weights which are optimal for the general case, the weights are varied until the the variance of the distribution of $\sum_i \omega_i \ (s_i + b_i)$ becomes minimal while keeping $\sum_i \omega_i s_i$ constant. The variance is given by

$$\sigma^2 = \sum_i \omega_i^2 \ (s_i + b_i) + \sum_l \ \left\{ \sum_i \omega_i \ (s_i \sigma_{li}^s + b_i \sigma_{li}^b) \right\}^2 ,$$

where l denotes the independent error sources which give rise to the systematic errors on the signal, $s_i \sigma_{l_i}^s$, and on the background, $b_i \sigma_{l_i}^b$, of the various channels. A unique solution, which minimises the variance, is guaranteed requiring $\omega_i \geq 0$. To fulfil this constraint, an unambiguously defined set of sub-channels has to be dropped.

A test-mass dependent 95% confidence level upper bound k_{95} is calculated for the quantity

$$k(m_{\mathrm{h}}) = \frac{\sigma_{\mathrm{hZ}}(m_{\mathrm{h}}) \times \mathrm{Br}(\mathrm{h} \to \mathrm{hadrons})}{\sigma_{\mathrm{HZ}}^{\mathrm{SM}}(m_{\mathrm{h}})}$$

where $\sigma_{\mathrm{HZ}}^{\mathrm{SM}}$ is the predicted SM cross-section for the Higgsstrahlung process. This bound is shown in Figure 6. In calculating this limit, the four-jet and tau channels were considered only for masses above 60 GeV/c^2 while the other channels contributed from 30 GeV/c^2 upwards. Between 12 and 30 GeV/c^2, only the data taken in the vicinity of $\sqrt{s} = 91$ GeV are used [4]. The region below 12 GeV/c^2 is covered by a decay mode independent Higgs boson search conducted by OPAL [35].

Limits on the cross-section σ for arbitrary $\mathrm{Br}(\mathrm{h} \to \mathrm{hadrons})$ or for arbitrary hZ coupling strength g_{hZ} can be derived using the expression

$$\sigma_{95} = k_{95} \times \sigma_{\mathrm{HZ}}^{\mathrm{SM}} \times \mathrm{Br}(\mathrm{h} \to \mathrm{hadrons}) \times (g_{\mathrm{hZ}}/g_{\mathrm{HZ}}^{\mathrm{SM}})^2,$$

provided that the effective hZ coupling has the SM Lorentz structure.

Assuming the hZ coupling predicted by the SM, a Higgs boson decaying only into hadronic final states ($k_{95}(m_{\mathrm{h}}) = 1$) is excluded for masses up to 104 GeV/c^2. For a Higgs boson also having the decay properties predicted by the SM, this limit is at 100 GeV/c^2.

5 Summary

A search has been performed for a hypothetical neutral scalar Higgs boson which is produced in Higgsstrahlung and which decays to hadrons of arbitrary flavour. The search is based on data collected by the OPAL experiment in e^+e^- collisions at centre-of-mass energies between 192 and 209 GeV. The results have been combined with earlier OPAL searches conducted at $\sqrt{s} \approx 91$ GeV and $\sqrt{s} = 189$ GeV. No significant excess has been observed over the background expected from Standard Model processes. A mass-dependent upper bound is set, at the 95% confidence level, on the product of the Higgsstrahlung cross-section and the hadronic branching ratio of the Higgs boson. For a Higgs boson which couples to the Z boson with Standard Model strength and which decays exclusively into hadronic final states, a flavour independent lower bound of 104 GeV/c^2 is obtained on the mass.

Acknowledgements

We particularly wish to thank the SL Division for the efficient operation of the LEP accelerator at all energies and for their close cooperation with our experimental group. In addition to the support staff at our own institutions we are pleased to acknowledge the
Department of Energy, USA,
National Science Foundation, USA,
Particle Physics and Astronomy Research Council, UK,
Natural Sciences and Engineering Research Council, Canada,
Israel Science Foundation, administered by the Israel Academy of Science and Humanities,
Benoziyo Center for High Energy Physics,
Japanese Ministry of Education, Culture, Sports, Science and Technology (MEXT) and a grant under the MEXT International Science Research Program,
Japanese Society for the Promotion of Science (JSPS),
German Israeli Bi-national Science Foundation (GIF),
Bundesministerium für Bildung und Forschung, Germany,
National Research Council of Canada,
Hungarian Foundation for Scientific Research, OTKA T-038240, and T-042864,
The NWO/NATO Fund for Scientific Research, the Netherlands.

References

[1] Reviewed in J.F. Gunion, H.E. Haber, G.L. Kane and S. Dawson, *The Higgs Hunter's Guide*, Addison-Wesley Publishing Co., 1990.

[2] W. Hollik, Z. Phys. **C32** (1986) 291; *idem* **C37** (1988) 569.

[3] X. Calmet and H. Fritzsch, Phys. Lett. **B496** (2000) 190;
C. Csaki, M.L. Graesser and G.D. Kribs,Phys. Rev. **D63** (2001) 065002;
G.F. Giudice, R. Rattazzi and J.D. Wells, Nucl. Phys. **B544** (1999) 3.

[4] OPAL Collab., G. Alexander et al., Z. Phys. **C73** (1997) 189.

[5] OPAL Collab., G. Abbiendi et al., Eur. Phys. J. **C18** (2001) 425.

[6] ALEPH Collab., A. Heister et al., Phys. Lett. **B544** (2002) 25.

[7] OPAL Collab., K. Ahmet et al., Nucl Instr. Meth. **305** (1991) 275;
M. Arignon et al., Nucl Instr. Meth. **313** (1992) 103;
D.G. Charlton, F. Meijers, T.J. Smith and P.S. Wells, Nucl Instr. Meth. **325** (1993) 129;
J.T.M. Baines et al., Nucl Instr. Meth. **325** (1993) 271;
M. Arignon et al., Nucl Instr. Meth. **333** (1993) 320;
B.E. Anderson et al., IEEE Transactions on Nuclear Science, **41** (1994) 845;
S. Anderson et al., Nucl Instr. Meth. **403** (1998) 326;
G. Aguillion et al., Nucl Instr. Meth. **417** (1998) 266.

[8] OPAL Collab., R. Akers et al., Phys. Lett. **B327** (1994) 397.

[9] OPAL Collab., K. Ackerstaff et al., Eur. Phys. J **C2** (1998) 213.

[10] P. Janot, in CERN Report 96-01, Vol. 2, p. 309 (1966).

[11] S. Jadach, B.F.L. Ward and Z. Was, Comp. Phys. Comm. **130** (2000) 260.

[12] T. Sjöstrand, Comp. Phys. Comm. **82** (1994) 74.

[13] J. Fujimoto et al., Comp. Phys. Comm. **100** (1997) 128.

[14] M. Skrzypek et al., Comp. Phys. Comm. **94** (1996) 216; *idem* Phys. Lett. **B372** (1996) 286.

[15] F.A. Berends, R. Pittau and R. Kleiss, Comp. Phys. Comm. **85** (1995) 437.

[16] S. Jadak, W. Placzek and B.F.L. Ward, in CERN Report 96-01, Vol. 2, p. 286 (1996); UTHEP-95–1001.

[17] S. Jadach, B.F.L. Ward and Z. Was, Comp. Phys. Comm. **79** (1994) 503.

[18] R. Engel and J. Ranft, Phys. Rev. **D54** (1996) 4244.

[19] G. Marchesini et al., Comp. Phys. Comm. **67** (1992) 465.

[20] J.A.M. Vermaseren, Nucl. Phys. **B229** (1983) 347.

[21] OPAL Collab., G. Alexander et al., Z. Phys. **C69** (1966) 543.

[22] J. Allison et al., Nucl. Instr. Meth. **A317** (1992) 47.

[23] OPAL Collab., G.Abbiendi et al., Eur. Phys. J.**C26** (2003) 479.

[24] OPAL Collab., G. Abbiendi et al., Eur. Phys. J. **C7** (1999) 407.

[25] OPAL Collab., K. Ackerstaff et al., Eur. Phys. J. **C2** (1998) 441.

[26] N. Brown and W.J. Stirling, Phys. Lett. **B252** (1990) 657;
idem, Z. Phys. **C53** (1992) 629.

[27] S. Catani and M.H. Seymour, Phys. Lett. **B378** (1996) 287.

[28] F.A. Berends and R. Kleiss, Nucl. Phys **B260** (1985) 32.

[29] ALEPH Collab., R. Barate et al., Phys. Lett. **B412** (1997) 173.

[30] M.W. Grünewald and G. Passarino, *Four-Fermion Production in Electron-Positron Collisions*, hep-ph/0005309.

[31] OPAL Collab., G. Alexander et al., Z. Phys. **C52** (1991) 175.

[32] OPAL Collab., K. Ackerstaff et al., Eur. Phys. J. **C1** (1998) 425.

[33] OPAL Collab., K. Ackerstaff et al., Eur. Phys. J. **C5** (1998) 19.

[34] R.D. Cousins and V.L. Highland, Nucl Instr. Meth. **A320** (1992) 331.

[35] OPAL Collab., G. Abbiendi et al., Eur. Phys. J. **C27** (2003) 311.

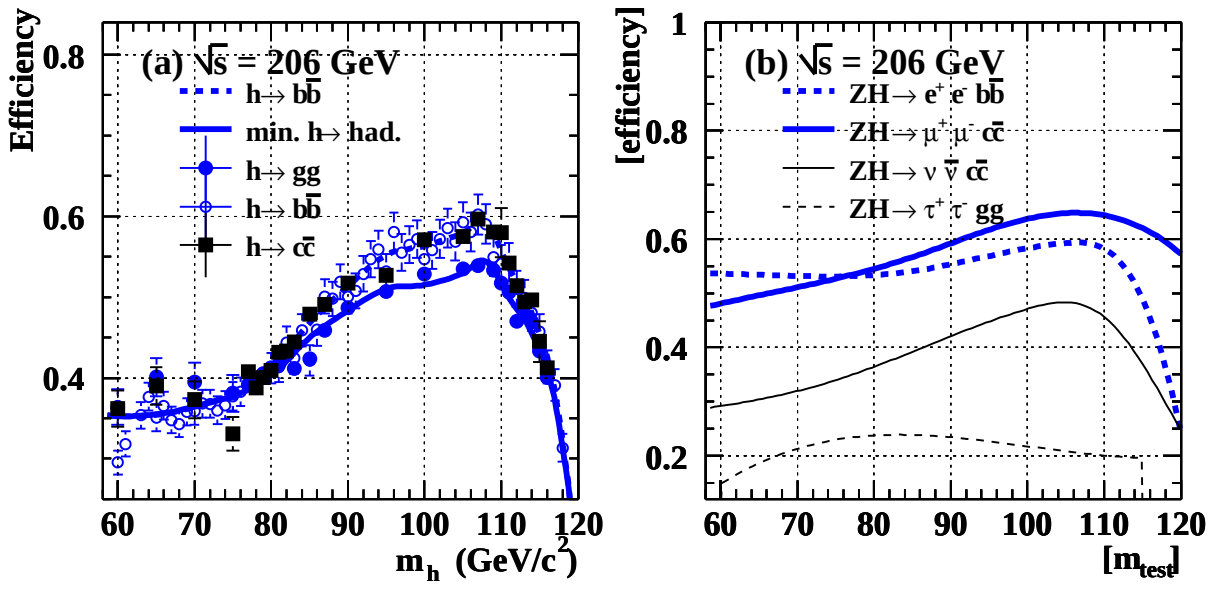

Figure 1: Selection efficiencies for the Higgsstrahlung process in the different search channels, at $\sqrt{s} = 206$ GeV. (a) Four-jet channel, flavour-dependence. The full line shows the result from a spline fit to the points with the lowest efficiency. (b) All but the four-jet channel. In each case, the lowest of the efficiencies over all hadron flavours is plotted.

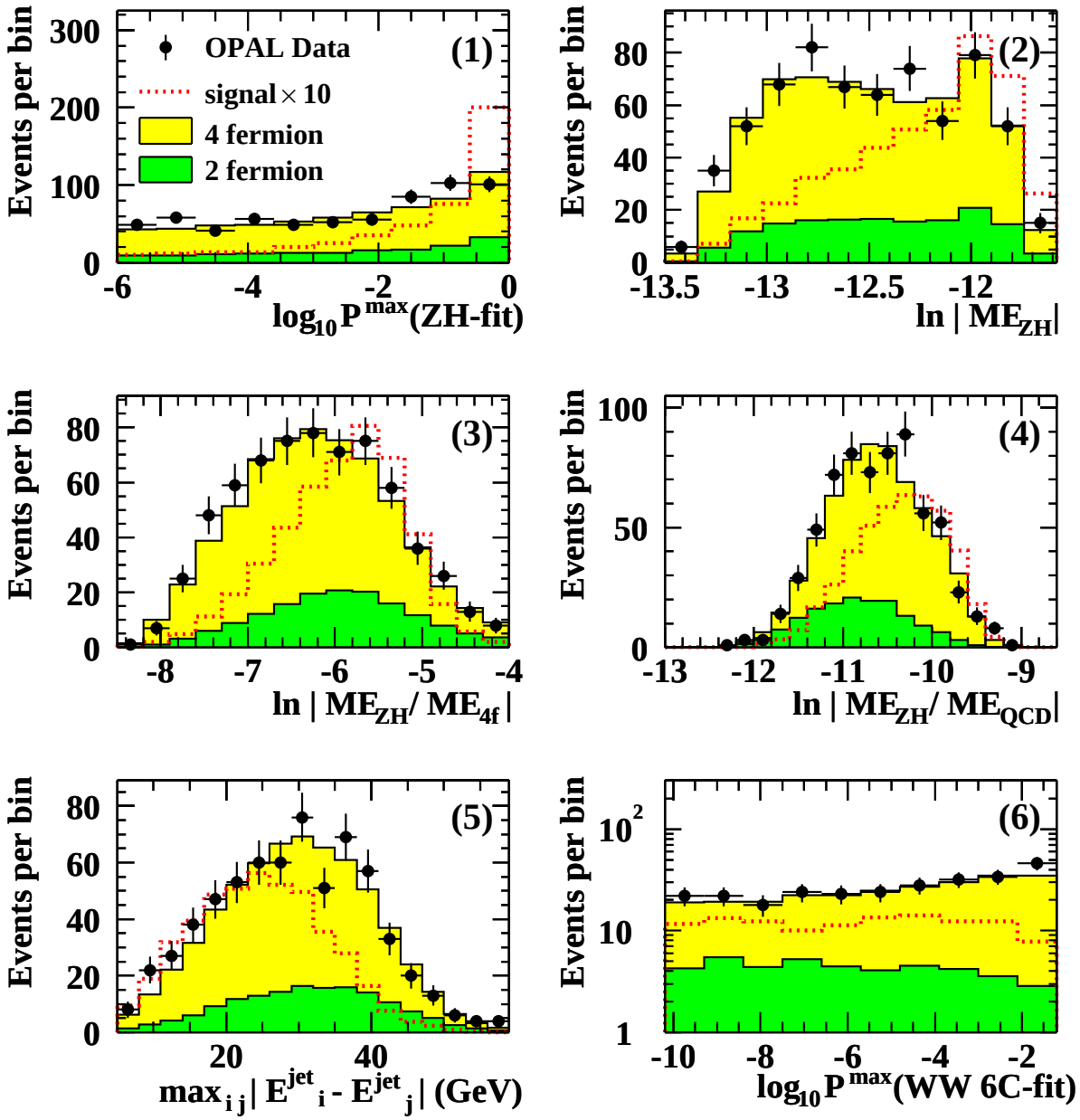

Figure 2: Distributions of discriminating variables which have been used in the construction of the signal likelihood in the four-jet channel, the test-mass m_{h} being fixed at 100 GeV/c^2. The dots with error bars show the data. The light and dark shaded histograms show the expected background from four- and two-fermion processes. The dashed histograms show the signal, scaled by a factor ten, expected for a Higgs boson of 100 GeV/c^2 mass, with hZ coupling predicted by the SM and decaying only into hadronic final states.

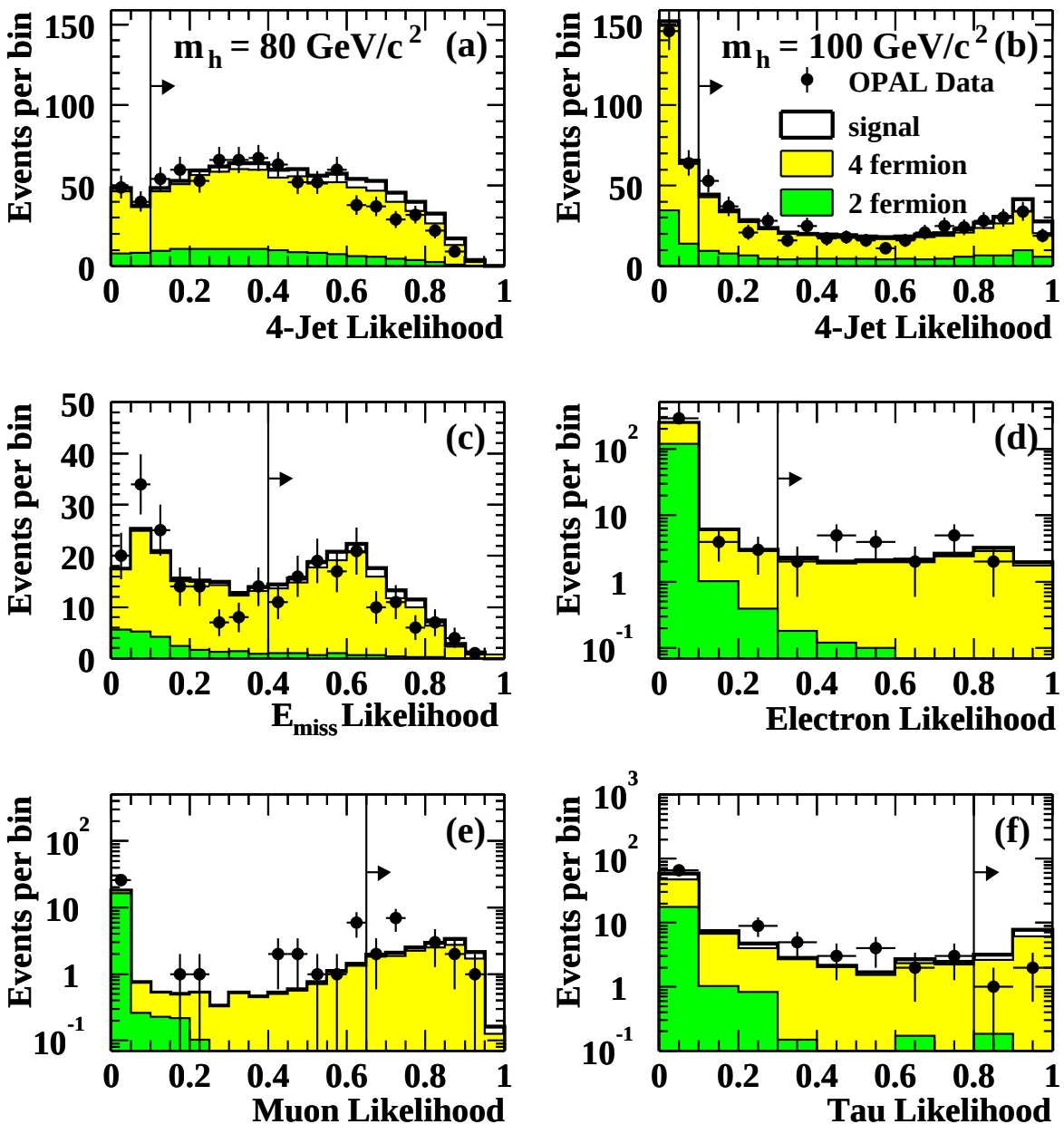

Figure 3: Distributions of the signal likelihoods for the searches in the (a-b) four-jet channel, (c) missing energy, (d) electron, (e) muon and (f) tau channels. In part (a) the test-mass m_{h} is fixed to 80 GeV/c^2; in all other parts it is at 100 GeV/c^2. The points with error bars represent the data. The light and dark shaded histograms show the expected background from four- and two-fermion processes. The white histograms added on top of the background contributions show the signal expected for a Higgs boson of 100 GeV/c^2 mass (80 GeV/c^2 in part (a)), with hZ coupling predicted by the SM and decaying only into hadronic final states. In each case, the vertical line indicates the final likelihood cut.

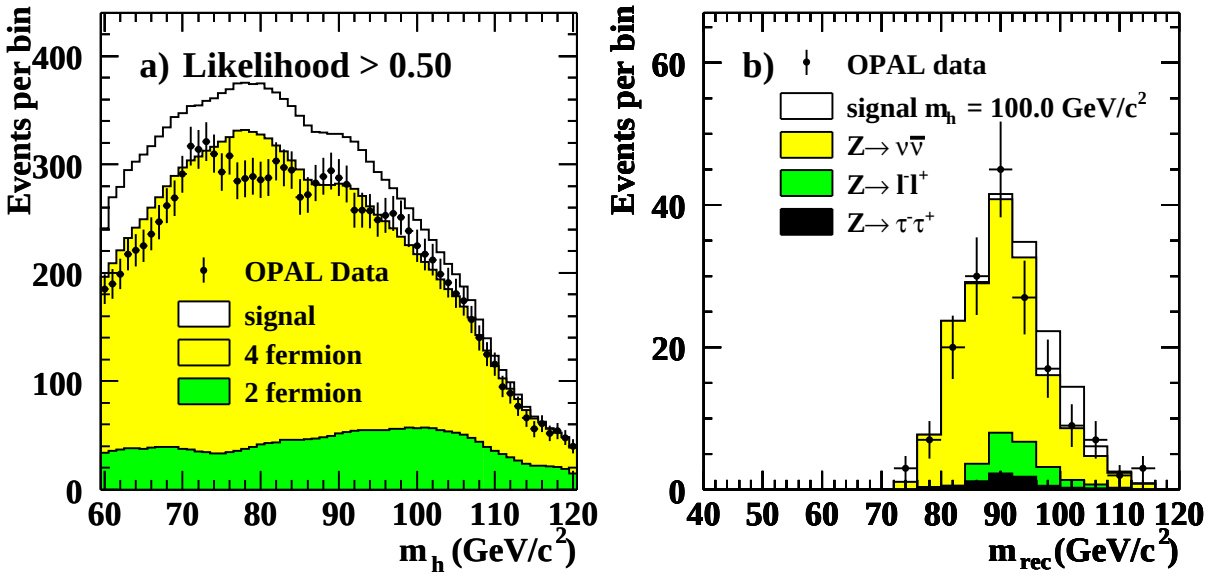

Figure 4: (a) Number of candidates selected in the four-jet channel as a function of the test-mass m_{h}, together with the predicted backgrounds and the signal from Higgsstrahlung added on top of the background. For the purpose of this figure the likelihood cut is raised to 0.5. (b) Combined distributions of the reconstructed Higgs boson mass in the missing energy, electron, muon and tau channels. For the signal, the Higgs boson mass is fixed at 100 GeV/c^2. In both parts of the figure, the hZ coupling predicted by the SM and 100% hadronic Higgs boson decays are assumed.

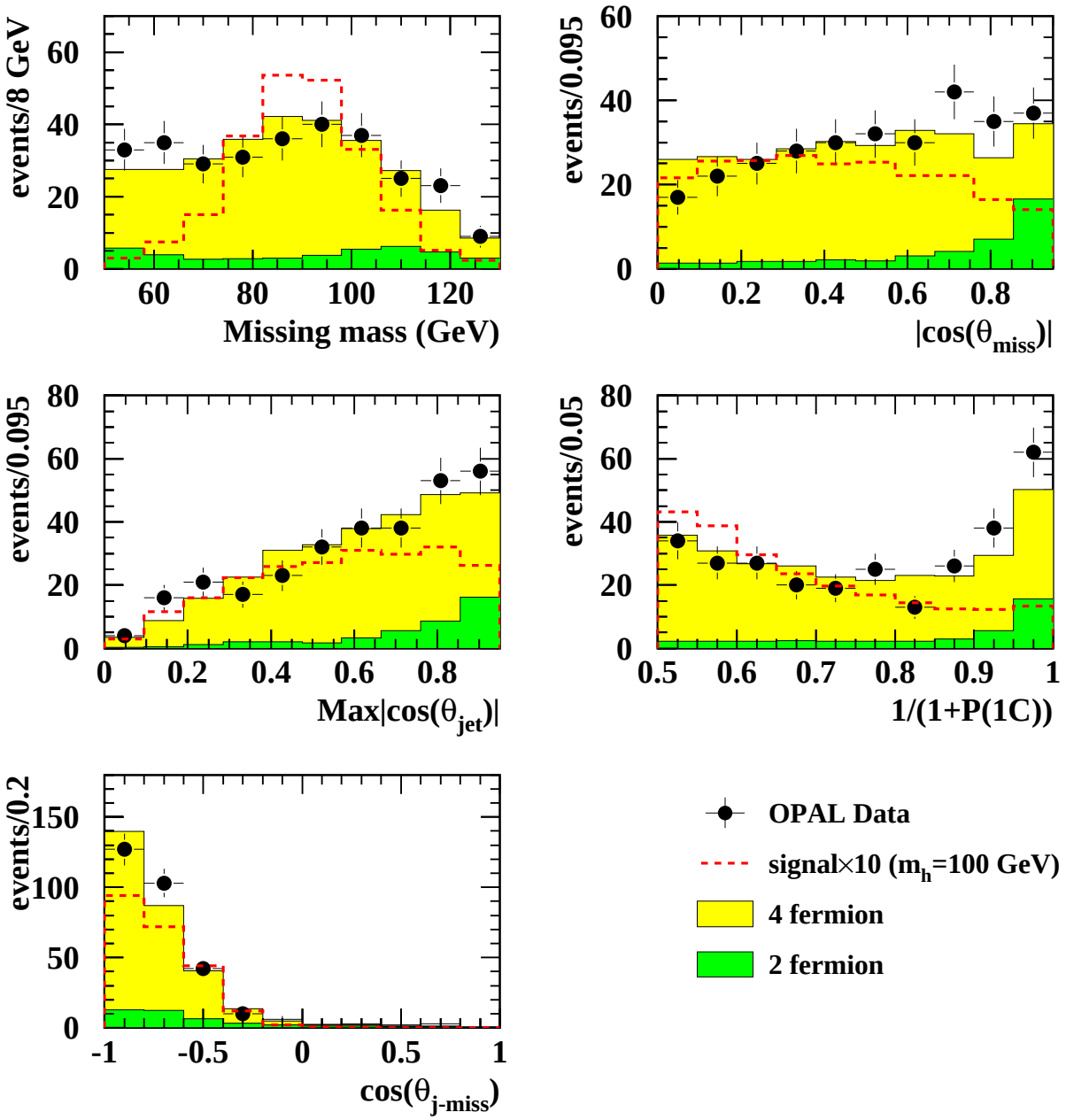

Figure 5: Distributions of the discriminating variables used to calculate the signal likelihood in the missing energy channel. The light and dark shaded histograms show the expected background from four- and two-fermion processes. The dashed histograms show the signal, scaled by a factor ten, expected for a Higgs boson of 100 GeV/c^2 mass, with hZ coupling predicted by the SM and decaying only into hadronic final states.

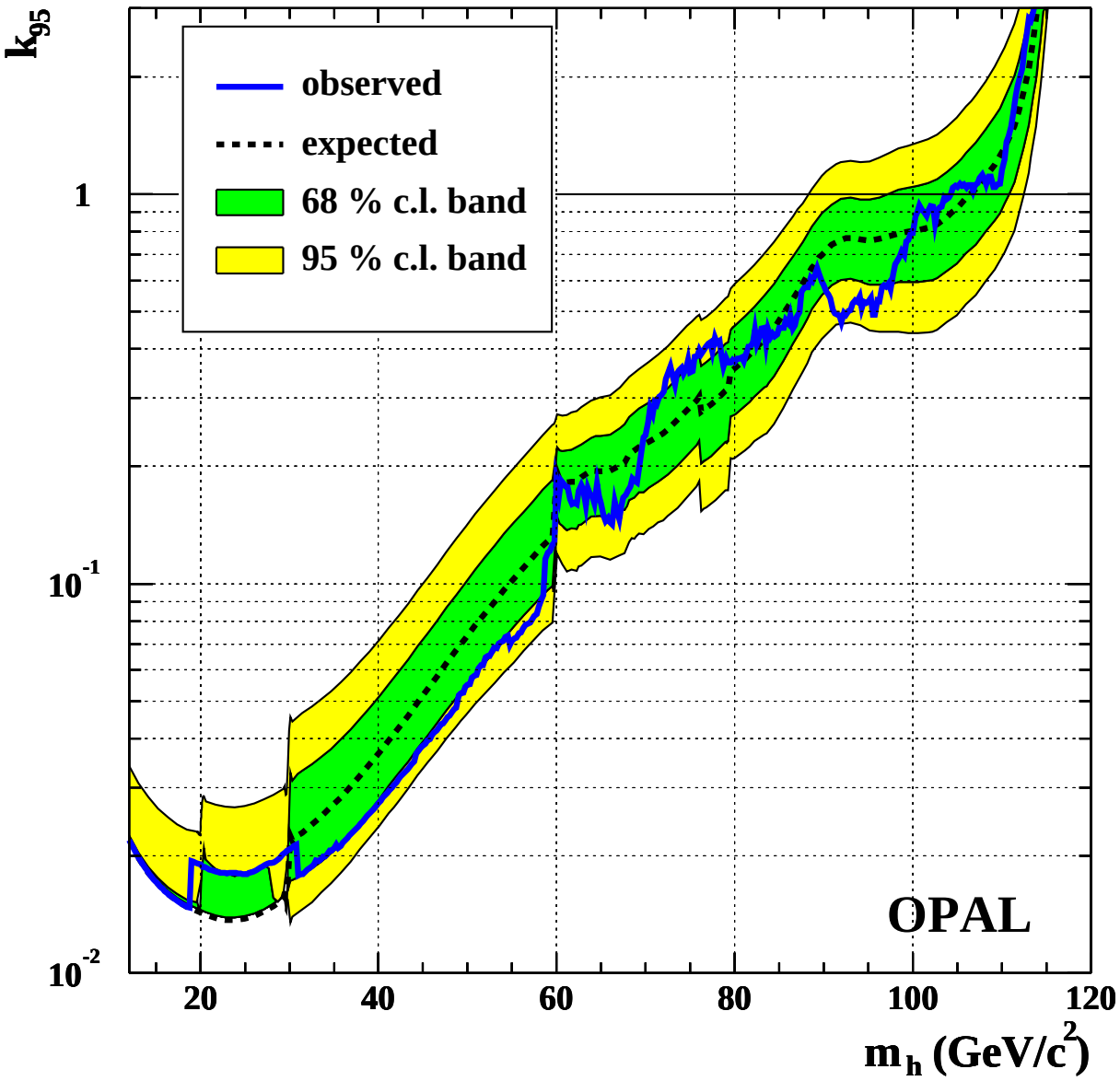

Figure 6: The 95% confidence level upper bound on the product k of the Higgsstrahlung cross-section and the hadronic decay branching ratio of the Higgs boson, divided by the Higgsstrahlung cross-section in the SM. The thick solid line shows the observed limit. The limit expected on average, in a large number of simulated experiments, in the absence of a Higgsstrahlung signal is indicated by the dashed line while the dark- and light-shaded areas show the 68% and 95% probability bands around the average.